Asian Journal of Atmospheric Environment
Vol. 2-1, pp.1-13, June 2008

Numerical Model for Stack Gas Diffusion in Terrain Containing Buildings -Application of Numerical Model to a Cubical Building and a Ridge Terrain-

Koichi Sada*, Takenobu Michioka and Yoichi Ichikawa

Environmental Science Research Laboratory, Central Research Institute of Electric Power Industry, 1464 Abiko, Abiko-shi, Chiba 270-1194, Japan

*Corresponding author. Tel: +81-4-7182-1181, E-mail: sada@criepi.denken.or.jp

ABSTRACT

A numerical simulation method has been developed to predict atmospheric flow and stack gas diffusion using a calculation domain of several km around a stack under complex terrain conditions containing buildings. The turbulence closure technique using a modified k-ε-type model under a nonhydrostatic assumption was used for the flow calculation, and some of the calculation grids near the ground were treated as buildings using a terrain-following coordinate system. Stack gas diffusion was predicted using the Lagrangian particle model, that is, the stack gas was represented by the trajectories of released particles. The numerical model was applied separately to the flow and stack gas diffusion around a cubical building and to a two-dimensional ridge in this study, before being applied to an actual terrain containing buildings in our next study. The calculated flow and stack gas diffusion results were compared with those obtained by wind tunnel experiments, and the features of flow and stack gas diffusion, such as the increase in turbulent kinetic energy and the plume spreads of the stack gas behind the building and ridge, were reproduced by both calculations and wind tunnel experiments. Furthermore, the calculated profiles of the mean velocity, turbulent kinetic energy and concentration of the stack gas around the cubical building and the ridge showed good agreement with those of wind tunnel experiments.

Key words: Atmospheric diffusion, Numerical analysis, Building, Terrain, Wind tunnel experiment

1. INTRODUCTION

Atmospheric flow and stack gas diffusion using a calculation domain of several km around a stack have been evaluated using wind tunnel facilities and numerical models. A turbulence closure model and a diffusion model, such as the Lagrangian particle model, have been applied in such numerical models. However, in these numerical models, the effect of buildings has not usually been considered; only the effect of the terrain has been considered because the released gas is usually located at a higher elevation, particularly for the case of buoyant stack gas. Furthermore, in such numerical models, the basic equations in the analysis used a terrain-following coordinate system, which meant that only terrain conditions were considered (e.g., Ichikawa and Sada, 2002, 2001; Yamada and Bunker, 1988). These models used a hydrostatic assumption; however, the turbulence caused by buildings was not accurately reproduced because the transport equation of vertical air flow was approximated to be the balance between vertical pressure gradient and air density, and accurate predictions of vertical air flow velocity and the increase in turbulence around buildings were impossible. To overcome these shortcomings, a flow and diffusion model for a terrain containing a building has been developed in this study, under a nonhydrostatic assumption using a terrain-following coordinate system.

The selection of a turbulence closure model for flow calculation was thus necessary, and a diffusion model was then selected for concentration calculations. Advanced turbulence analysis techniques, such as large-eddy simulation for the turbulent diffusion of stack gas around buildings (Sada and Sato, 2002; Henn and Sykes, 1992) and Reynolds stress turbulence closure modelling of a terrain under a nonhydrostatic assumption (Mengelkamp, 1991; Gross and Wippermann, 1987), require large amounts of computational resources. An additional reason for the selection of a turbulence closure model in this study was that the variations of calculation results were not large with the turbulence closure model when the calculation domain includes many buildings has been resolved using fine calculation grids (e.g., Yoshizawa *et al.*,

1995; Takakura *et al.*, 1993). For these reasons, a k-ε-type model under a nonhydrostatic assumption was applied. Furthermore, the turbulent kinetic energy obtained using a standard k-ε model is much higher than that obtained by wind tunnel experiments, particularly upstream of a building roof edge; thus, a modified model was selected as a flow model (Tsuchiya *et al.*, 1997). Then, stack gas diffusion in this study was predicted using the Lagrangian particle model, that is, the stack gas was represented by the trajectories of released particles. This was because the effect of the numerical viscosity around a stack is not negligible when using finite-difference techniques for concentration calculation with the coarse calculation grids, but is negligible when the Lagrangian particle model is used, and also because of its calculation accuracy near the stack. Furthermore, the turbulence caused by buildings and the terrain is directly considered in the stack gas diffusion calculation, because its calculated velocity and turbulent kinetic energy, as well as its dissipation rate, are used in diffusion calculations in the Lagrangian particle model. A Lagrangian model (Thomson, 1987) that is superior to conventional Lagrangian particle models in its applicability to non-Gaussian and inhomogeneous turbulent fields and in its use of Gaussian random numbers was adopted in this study. This model has been applied to the analysis and calculation of stack gas diffusion under a convective boundary layer (Weil, 1990; Luhar and Britter, 1989) and a complex terrain (Ichikawa and Sada, 2001). However, the turbulence in the Lagrangian particle model used in this study is treated as Gaussian mentioned later in section 2.2.

A flow and diffusion model around buildings and terrain using the modified k-ε model and the Lagrangian particle model was developed, and the model was applied separately to a cubical building and to a two-dimensional ridge terrain in this study before being applied to an actual terrain containing buildings in the subsequent study (Sada *et al.*, 2006). The calculated flow and stack gas diffusion results were compared with those obtained by wind tunnel experiments. From these comparisons between experimental and calculated results, the prediction accuracy of the developed numerical model was verified.

2. NUMERICAL MODEL

2.1 Flow

Flow fields were calculated using the turbulence closure model, that is, the modified k-ε model (Murakami, 1997; Tsuchiya *et al.*, 1997), to evaluate the turbulent quantities around a cubical building and a ridge. Because the terrain altitude varies, model equations were transformed to a generalized coordinate system. Furthermore, the calculation grids neighboring the ground where the building was located were treated as a bluff body to reproduce the shape of the building under a generalized coordinate system, as mentioned later. The physical coordinate x was transformed to the calculation coordinate ξ. The continuity equation, transport equations for momentum, turbulent kinetic energy and its dissipation rate to be solved in this study were

$$\frac{1}{J}\frac{\partial JU^{\alpha}}{\partial \xi^{\alpha}}=0, \tag{1}$$

$$\frac{\partial u_i}{\partial t}+\frac{1}{J}\frac{\partial}{\partial \xi^{\alpha}}(JU^{\alpha}u_i) =-\frac{1}{\rho J}\frac{\partial}{\partial \xi^{\alpha}}(JA_i^{\alpha}p)+\frac{1}{J}\frac{\partial}{\partial \xi^{\alpha}}\{2(\nu_t+\nu)JA_j^{\alpha}D_{ij}\}, \tag{2}$$

$$\frac{\partial k}{\partial t}+\frac{1}{J}\frac{\partial}{\partial \xi^{\alpha}}(JU^{\alpha}k) =P_k-\varepsilon+\frac{1}{J}A_i^{\beta}\frac{\partial}{\partial \xi^{\beta}}\left\{J\left(\frac{\nu_t}{\sigma_k}+\nu\right)A_i^{\alpha}\frac{\partial k}{\partial \xi^{\alpha}}\right\} \tag{3}$$

and

$$\frac{\partial \varepsilon}{\partial t}+\frac{1}{J}\frac{\partial}{\partial \xi^{\alpha}}(JU^{\alpha}\varepsilon)=(C_{\varepsilon 1}P_k-C_{\varepsilon 2}\varepsilon)\frac{\varepsilon}{k} +\frac{1}{J}A_i^{\beta}\frac{\partial}{\partial \xi^{\beta}}\left\{J\left(\frac{\nu_t}{\sigma_\varepsilon}+\nu\right)A_i^{\alpha}\frac{\partial \varepsilon}{\partial \xi^{\alpha}}\right\}, \tag{4}$$

respectively. Here, D_{ij} is the rate-of-strain tensor $(\partial u_i/\partial x_j+\partial u_j/\partial x_i)/2$, and the mean velocity of the physical domain u_i was transformed to the calculation domain U^i using $U^{\alpha}=(\partial \xi^{\alpha}/\partial x^i)u_i=A_i^{\alpha}u_i$. The buoyancy effect caused by stable and unstable stratifications in the atmosphere and the Coriolis force were disregarded, as in wind tunnel experiments. Next, the eddy viscosity in the modified k-ε model was determined. With reference to the standard k-ε model of $\nu_t=C_\mu k^2/\varepsilon$, its formation was given as

$$\nu_t=C_\mu^*\frac{k^2}{\varepsilon}, \tag{5.1}$$

where

$$C_\mu^*=\begin{cases} C_\mu\cdot\Omega/S : \Omega<S \\ C_\mu \quad\quad : \Omega\geq S. \end{cases} \tag{5.2}$$

On the basis of the above-mentioned formation of eddy viscosity, the large turbulent kinetic energies calculated around a building using the standard k-ε model, particularly upstream and at elevated corners of the building, were reduced. The strain of velocity was increased, and eventually the ratio of Ω/S became

less than unity upstream and at elevated corners of the building. Because of this, eddy viscosity decreased with the model constant C_μ^*, from Eq. (5.1), upstream at elevated corners of the building, and the production terms in the turbulent kinetic energy transport equation were predicted to eventually attenuate.

The calculation grids were formed using the so-called terrain-following coordinate system to resolve terrain conditions (e.g., Ichikawa and Sada, 2002, 2001; Yamada and Bunker, 1988), that is, only vertical linear interpolation was necessary in the generation of the grids. The shape of the building on flat ground reproduced using the calculation grids neighboring the ground surface was treated as a bluff body. Furthermore, zero-gradient pressure in the direction normal to the building surfaces was employed in the momentum transport equation. The inlet conditions for velocity and turbulent kinetic energy were set on the basis of the results obtained in wind tunnel experiments, and a free-exit boundary condition, namely, a zero gradient in the mean flow direction, was used at the position of outflow. A first-order upwind differential scheme was adopted for the convection terms of the conservation equations, and the Euler explicit scheme was used for the time difference. The wall function techniques of velocity, turbulent kinetic energy and its dissipation rate,

$$\frac{u_w}{u_*}=\frac{1}{\kappa}ln\left(\frac{z_n+z_0}{z_0}\right), \tag{6.1}$$

$$\frac{k_w}{u_*^2}=\frac{1}{C_\mu^{1/2}}, \tag{6.2}$$

and

$$\frac{\varepsilon_w}{u_*^3}=\frac{1}{\kappa z_n}, \tag{6.3}$$

respectively, were applied to not only the flat ground including the ridge surface, but also the building surfaces. In the above-mentioned equations, the local wind profile is considered to be logarithmic, and empirical relations were assumed for turbulent kinetic energy and its dissipation rate, where the subscript w indicates the values of the neighboring grids to the ground and building surfaces, and z_n is the distance from the ground and building surfaces to the defining point of the variables.

2.2 Concentration

The governing equations of the Lagrangian particle model (Thomson, 1987) are stochastic diffusion equations representing the random motion of a particle as

$$d\boldsymbol{u}^i=a^i(\boldsymbol{x},\boldsymbol{u},t)dt+b^{ij}(\boldsymbol{x},\boldsymbol{u},t)d\xi^j \tag{7}$$

and

$$d\boldsymbol{x}=\boldsymbol{u}dt, \tag{8}$$

where $d\xi^j$ is the increment in the Wiener process with mean zero and the variance dt. The coefficients a and b describe the effects of the particle and random motion, namely, the dynamic characteristics and noise, respectively. Thomson proposed the following equation to derive the coefficient for a Gaussian turbulence,

$$a^i=-B^{ij}(V^{-1})^{jk}(u^k-U^k)+\phi^i/g_a, \tag{9}$$

$$\begin{aligned}\frac{\phi^i}{g_a}=&\frac{1}{2}\frac{\partial V^{il}}{\partial x^l}+\frac{\partial U^i}{\partial t}+U^l\frac{\partial U^i}{\partial x^l}\\&+\left\{\frac{1}{2}(V^{-1})^{lj}\left(\frac{\partial V^{il}}{\partial t}+U^m\frac{\partial V^{il}}{\partial x^m}\right)+\frac{\partial U^i}{\partial x^j}\right\}(u^j-U^j)\\&+\frac{1}{2}(V^{-1})^{lj}\frac{\partial V^{il}}{\partial x^k}(u^j-U^j)(u^k-U^k),\end{aligned} \tag{10}$$

and

$$2B^{ij}=\delta^{ij}C_0\varepsilon, \tag{11}$$

where $B^{ij}=b^{ik}b^{jk}/2$, δ_{ij} is the Kronecker delta, and C_0 is the model constant; its value has been examined by theoretical analysis, calculation and the comparison of wind tunnel and field observation data. Despite many investigations of C_0, its exact value has not yet been determined, but it is between 1 and approximately 10 (Ichikawa and Sada, 2002, 2001). In this study, this model constant was examined by calculations using flow calculation results, and a suitable value of the model constant $C_0=5$ was selected.

Because the diffusion calculations were performed separately for the cubical building and the ridge terrain, each released particle was assumed to be reflected perfectly at not only the ground including the ridge surface, but also the building surface. The position of the particle after reflection, $\boldsymbol{x}'$ in vector notation, was calculated as

$$\boldsymbol{x}'=\boldsymbol{x}-2\boldsymbol{n}\{\boldsymbol{n}\cdot(\boldsymbol{x}-\boldsymbol{x}_p)\}, \tag{12.1}$$

where $\boldsymbol{x}$ is the position of the particle in the case of no reflection, and $\boldsymbol{x}_p$ is the position of the reflection point. The velocity vector $\boldsymbol{u}'$ of the particle after reflection was calculated as

$$\boldsymbol{u}'=\boldsymbol{u}-2\boldsymbol{n}(\boldsymbol{n}\cdot\boldsymbol{u}), \tag{12.2}$$

where $\boldsymbol{u}$ is the velocity vector of the particle in the case of no reflection.

3. WIND TUNNEL EXPERIMENTS

Wind tunnel experiments were conducted using the

facility at the Komae Research Lab. of CRIEPI to obtain the data used for comparison with the calculation results. The wind tunnel had a 3-m-wide, 1.5-m-high and 20-m-long test section. To form a thick turbulent boundary layer on the wind tunnel floor, a free stream velocity of U=2.0 m/s was employed, and the turbulence grid and stimulators on the floor were set at the entrance of the test section. The model stack was set 4 m leeward of the entrance of the test section. Using this experimental setup, flow and stack gas diffusion characteristics similar to those of the atmosphere (Kakishima *et al.*, 1985) under a flat-plate condition were confirmed assuming constant length ratios for the cubical building and the ridge terrain. A cubical building (1 : 100 length ratio) and a ridge (1 : 1,000 length ratio) were separately placed on the flat floor in the test section. Though the different length ratios were used in the wind tunnel experiments, the vertical plume spreads under a flat-plate condition in the wind tunnel under the length ratio of 1 : 1,000 ranged between stabilities C and D, as mentioned later in Fig. 2, and close to the stability D near the stack under the length ratio of 1 : 100. The mean and fluctuations of velocity were measured using a laser Doppler velocimeter. Ethylene (C_2H_4), which has a buoyancy similar to that of air, was released from the model stack as the tracer gas using a Γ-type model stack (Sada, 1996; Kakishima *et al.*, 1985). Sampling gas was collected at various locations, and its concentration was measured using flame ionization detectors.

4. CALCULATION RESULTS AND DISCUSSION

4.1 Flat Plate

The calculation domain under the flat-plate condition was 8 km in the streamwise direction (2 km and 6 km from the stack in the windward and leeward directions, respectively), and 3 km and 2 km in the lateral and vertical directions, respectively. This calculation domain was divided by grids following the terrain-following coordinate system, however, grid lines were orthogonal to each other, similar to the rectangular coordinate system, because of the flat-plate condition. The streamwise and lateral widths of grids, namely, in the x and y directions, were set to 200 m throughout the calculation domain. The vertical widths of the grids were set to 10 m on the ground surface, and smoothly increased with height up to approximately 200 m. This calculation domain was divided into 40, 15 and 20 grids in the x, y and z directions, respectively.

The mean wind velocity, and the lateral and vertical

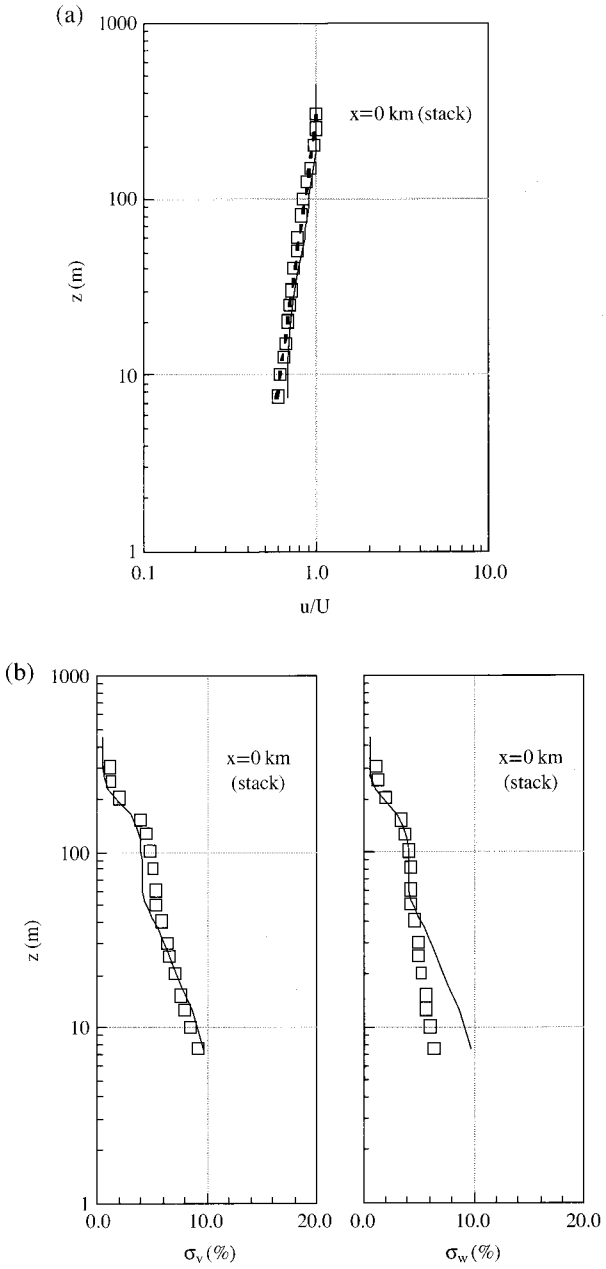

Fig. 1. Flow field at stack position under flat-plate condition under length ratio of 1 : 1,000. (a) Mean velocity. Squares, the solid line and the broken line indicate the results of wind tunnel experiments, calculations and the 1/7 power law, respectively. (b) Lateral and vertical turbulence intensities σ_v and σ_w are normalized by local velocity. Squares and lines indicate the results of wind tunnel experiments and calculations, respectively.

turbulence intensity profiles at the stack position are shown in Fig. 1. The boundary layer thickness was approximately 300 m, and the stack gas release height was within the boundary layer. The power law $u \propto z^p$

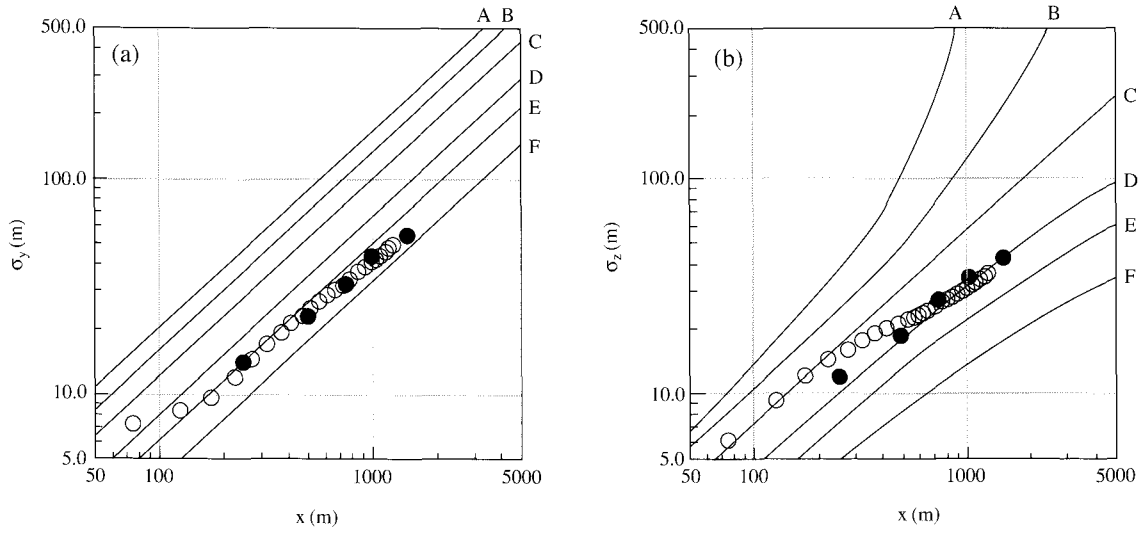

Fig. 2. Plume spreads under flat-plate condition and comparison with P-G chart. The plume spreads under highly unstable, unstable, slightly unstable, neutral, stable and highly stable atmospheric conditions are indicated by A, B, C, D, E and F, respectively. Open circles and lines indicate the calculated results and profiles of the P-G chart, respectively. Close circles indicate the wind tunnel results of the length ratio of 1 : 1,000. (a) Lateral and (b) vertical plume spreads for an elevated source, H=25 m.

was applied to the vertical velocity profile, and its coefficient p was approximately 1/7, which was the same as that obtained under the flat-plate condition in the atmosphere. Turbulence intensities increased in the vicinity of the ground within the turbulent boundary layer. Although almost the same profiles of lateral turbulence intensity were obtained for calculations and experiments, larger values were obtained for vertical turbulence intensity in the vicinity of the ground in the calculations. This was due to the isotropic features of the modified k-ε model used in this study, in which almost the same values were calculated for the lateral and vertical directions.

Then, the similarity between the calculated results and those obtained in the atmosphere was examined, and the results of plume spreads are shown in Fig. 2. The vertical plume spread ranged between stabilities C and D in the so-called P-G chart (Pasquill, 1974), which is similar to the case of neutral atmospheric conditions, and also similar to the wind tunnel of the ridge, viz., the length ratio of 1 : 1,000. The vertical plume spread in the wind tunnel of the building, viz., the length ratio of 1 : 100, were slightly smaller than the stability D, however, close to the stability D near the stack, Although the lateral plume spread approached stability D in the vicinity of the stack, the spread was smaller than that in the atmosphere under the neutral and near stable conditions far from the stack. This was due to the meandering of the plume in the atmosphere not being reproduced. The smaller spread of lateral plume profile far from the stack was also obtained in wind tunnel experiments (Kakishima *et al.*, 1985).

4.2 Building

The calculation domain was first set without a cubical building and was 200 m in the streamwise and lateral directions and 100 m in the vertical direction, and the grids in the vertical direction were formed by applying linear interpolation between the top of the calculation domain and the ground using the terrain-following coordinate system. The widths of the grids in all directions were set at 5 m and were not varied. Thus, the calculation domain was divided into 40 grids in the streamwise and lateral directions and 20 grids in the vertical direction. The formed grid lines were orthogonal to each other, similar to the rectangular coordinate system, because the terrain altitude was not varied within the calculation domain. Then, a cubical building with height and side lengths of 20 m was set at the center of the calculation domain on the ground surface. This building was constrained in $4 \times 4 \times 4$ calculation grids in the streamwise, lateral and vertical directions, and was treated as a bluff body. The center of the building was set as the coordinate origin, x=0 m, and the model stack was located on the center of the building roof (see Fig. 3(c)).

The calculated profiles of mean velocity and velocity vectors are shown in Fig. 3, turbulent kinetic energy is shown in Fig. 4, and lateral and vertical turbulence intensities are shown in Fig. 5. The vertical profiles of wind velocity smoothly varied with height

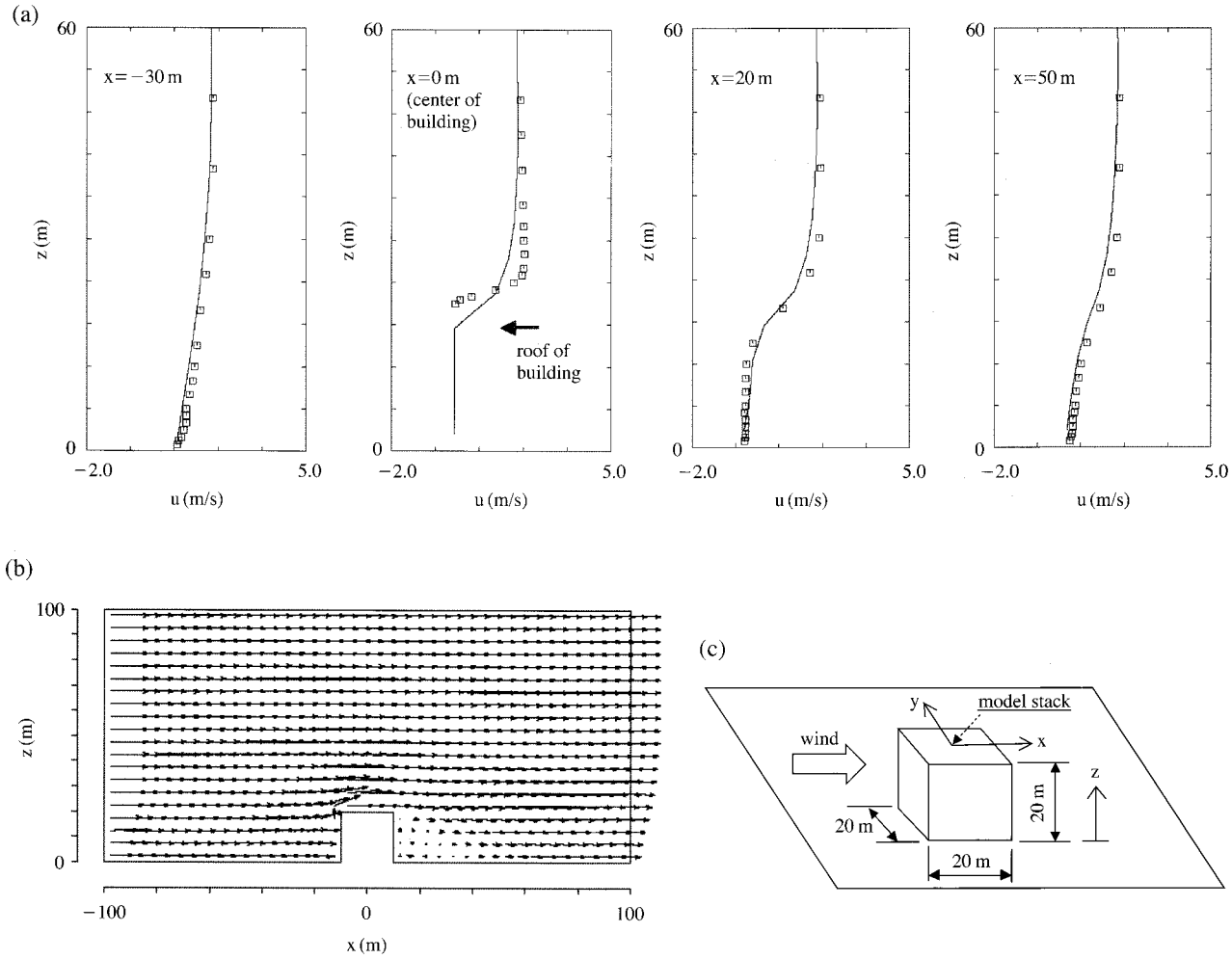

Fig. 3. (a) Mean velocity at y=0 m, the center position of the cubical building. The solid lines and squares indicate the results of calculations and wind tunnel experiments, respectively. (b) Velocity vectors around the cubical building at y=0 m. (c) The configuration of the building and stack.

from the ground and were similar to results obtained under the flat-plate condition windward of the building at x=−30 m. The flow directions changed to upward and the wind velocity increased due to the existence of the building. Although these features of wind velocity were obtained for both calculations and experiments, the calculated wind velocity increased slowly with height compared with experimental results at x=0 m. A reversed flow, indicated by negative values of wind velocity, was obtained behind the building near the ground at x=20 m, and a cavity region appeared, as shown in Fig. 3(b). The reversed flow was not observed far from the building at x=50 m. These features of wind velocity were observed in both calculations and experiments, and the profiles of wind velocity coincided, as shown in Fig. 3(a) for x=20 and 50 m.

Larger calculated values of turbulent kinetic energy than those in experiments were obtained windward of the building at x=−30 m. This was due to the large calculated values of turbulent kinetic energy around the upwind corners of the building, even when using the modified version of the k-ε closure model. On the other hand, the calculated values of turbulent kinetic energy in the vicinity of the building roof at x=0 m and z=21-24 m, were smaller than those in experiments. This might be due to the coarse grid resolution used in the calculations, and the small cavity region on the building roof, often observed in experiments (Murakami *et al.*, 1998), was not apparent, as shown in Fig. 3(b). Such a cavity region on the building roof might cause an increase in the velocity strain, and consequently an increase in turbulent kinetic energy in experiments, as shown in Fig. 4 at x=0 m and z=

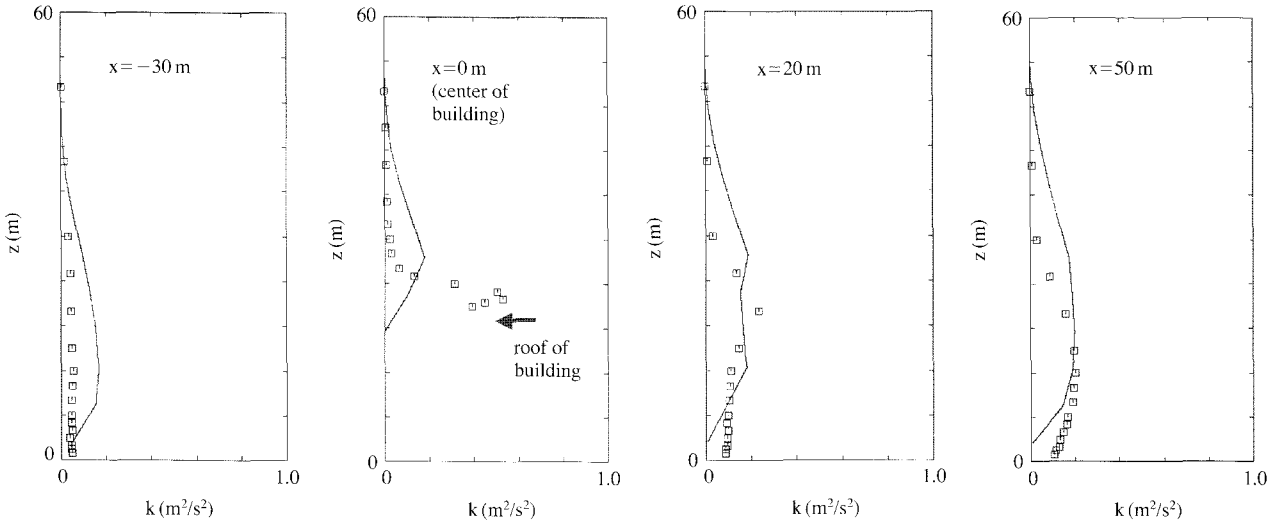

Fig. 4. As Fig. 3(a) but for turbulent kinetic energy.

21-24 m. Although some discrepancies in turbulent kinetic energy were obtained by calculation, calculated profiles were similar to those of experiments, also for profiles leeward of the building at x=20 and 50 m. The calculated turbulence intensities in the lateral and vertical directions had almost the same values due to the isotropic features of the modified k-ε model. On the other hand, turbulent mixing become activated due to the existence of the building, and the turbulence intensities obtained in experiments increased in all directions. Eventually, turbulence intensities in experiments showed similar profiles in the lateral and vertical directions. Because of this, the calculated profiles of turbulence intensities were almost the same as the experimental results, as shown in Fig. 5.

The calculated mean concentration in the vertical and lateral directions, normalized by the source strength and the free stream velocity, are shown in Figs. 6 and 7, respectively. Because the tracer gas was released from the elevated position of z=20 m, the plume center was also calculated at an elevated position of z=20 m, as shown in Fig. 6(a). A narrow spread of the concentration was calculated near the stack at x= 20 m, and increases in plume spread were calculated at leeward positions, x=30 and 50 m. Because of this plume spread, the maximum concentration at the plume center decreased in the leeward direction, as shown in Fig. 6(a). Furthermore, the plume was calculated to diffuse partially into the cavity region behind the building at x=20 m and reach the ground surface. A comparison of these features of calculated concentration in the vertical and lateral directions with those obtained in experiments reveals some discrepancies. The maximum calculated value of concentration at x=20 m was larger than that obtained in experiments, as shown in Figs. 6 and 7. This might be due to the less active diffusion of the plume in calculations, caused by the small calculated turbulence intensities on the building roof around z=21-24 m, as shown in Fig. 5. Although there were some discrepancies between the results of the calculations and experiments, the regions in which these discrepancies were observed were limited; otherwise, there was generally good agreement.

4.3 Ridge

The dimensions of calculation domain were 2,300, 1,200 and 3,000 m in the streamwise, lateral and vertical directions, respectively, and the calculation grids in the vertical direction were made by applying linear interpolation between the top of the calculation domain and the ground including the ridge surface. The widths of the grids in the streamwise and lateral directions were 10 m and these widths were not varied. On the other hand, the widths of the grids in the vertical direction were 10 m on the ground and increased with height up to approximately 200 m at the entrance of the calculation domain. The ridge crest was located at x=0 m and was 1,100 m leeward from the entrance of the calculation domain. The altitude of the ridge crest was 135 m, and its cross section was triangular with a base extending 300 m in both the windward and leeward directions from the ridge crest. Thus, the terrain altitude varied for x=−300 m to 300 m (see Fig. 8(c)), and terrain did not vary in the lateral direction, viz., the ridge terrain was two dimensional. The calcula-

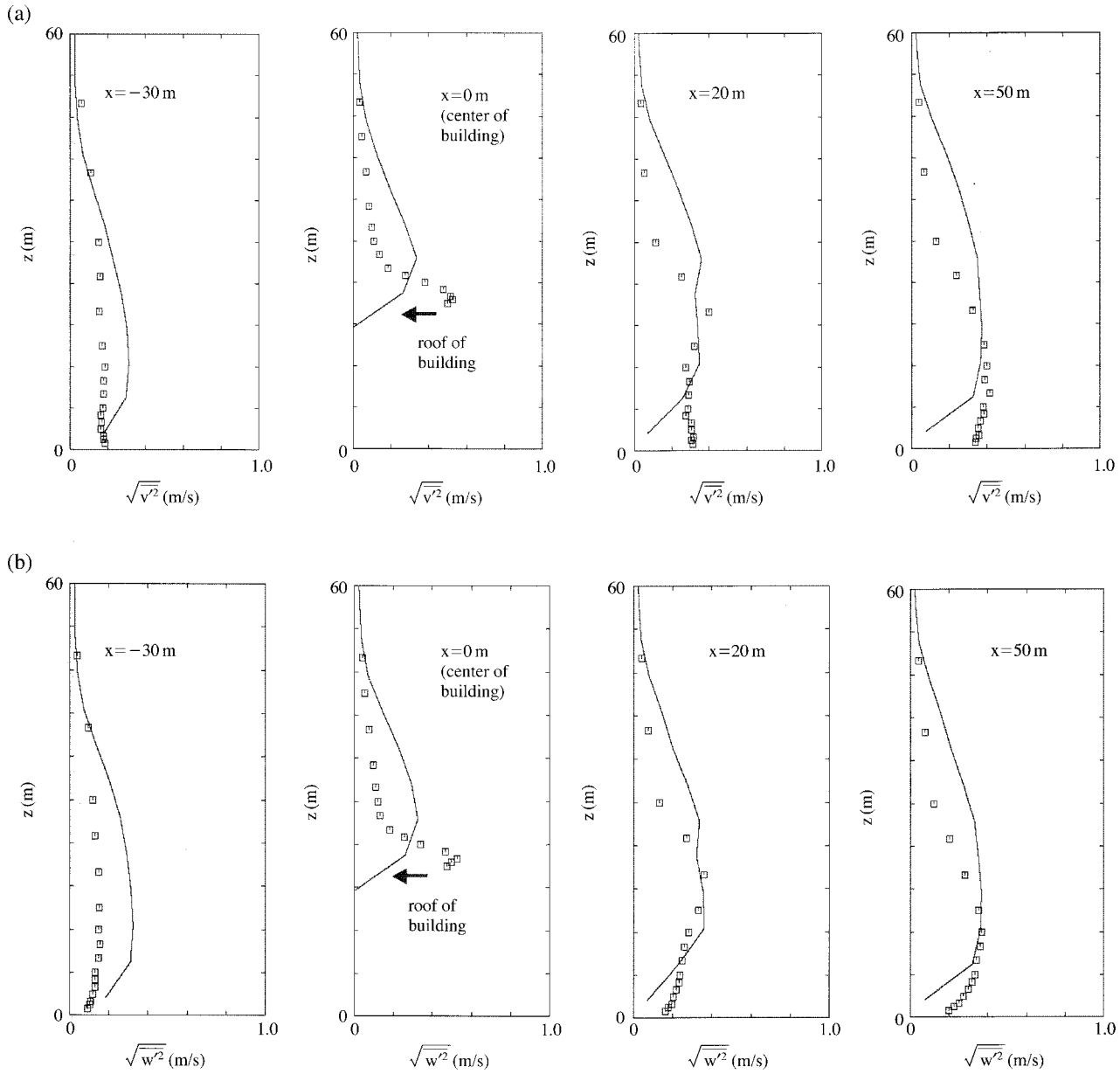

Fig. 5. As Fig. 3(a) but for (a) lateral turbulence intensity and (b) vertical turbulence intensity.

tion domain was divided by 230, 120 and 50 grids in the streamwise, lateral and vertical directions, respectively. The model stack was located at x=−1,000 m at an elevated position of z=50 m.

The calculated mean velocity and velocity vectors are shown in Fig. 8, and the turbulent kinetic energy is shown in Fig. 9. The vertical profiles of wind velocity smoothly varied with height from the ground windward of the ridge at x=−1,000 and −300 m. The flow directions became upward and wind velocity increased at x=0 m due to the ridge, as shown in Fig. 8(a) and (b). These features were observed in both calculations and experiments. However, there was a marked increase in wind velocity at x=0 m in the calculation, and the calculated values of velocity were larger than those in the experiments in the vicinity of the ground. This might imply that the terrain had a significant effect on the calculation results obtained using the model developed in this study, particularly around the ridge crest where the spatial variation of turbulence was large, for instance, the flow direction changed from upward to downward at the ridge crest.

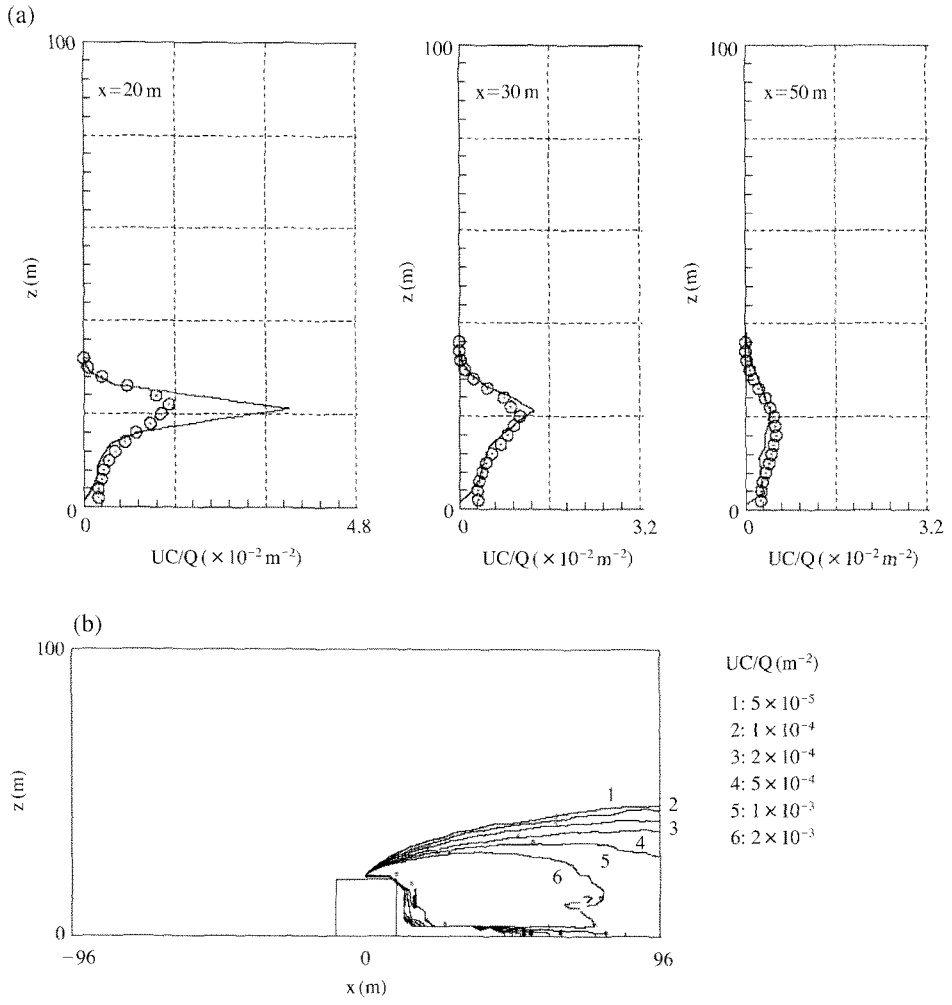

Fig. 6. (a) Mean concentration at y=0 m, the center position of the cubical building. The solid lines and squares indicate the results of calculations and wind tunnel experiments, respectively. (b) Contour lines of mean concentration on xz cross section at y=0 m.

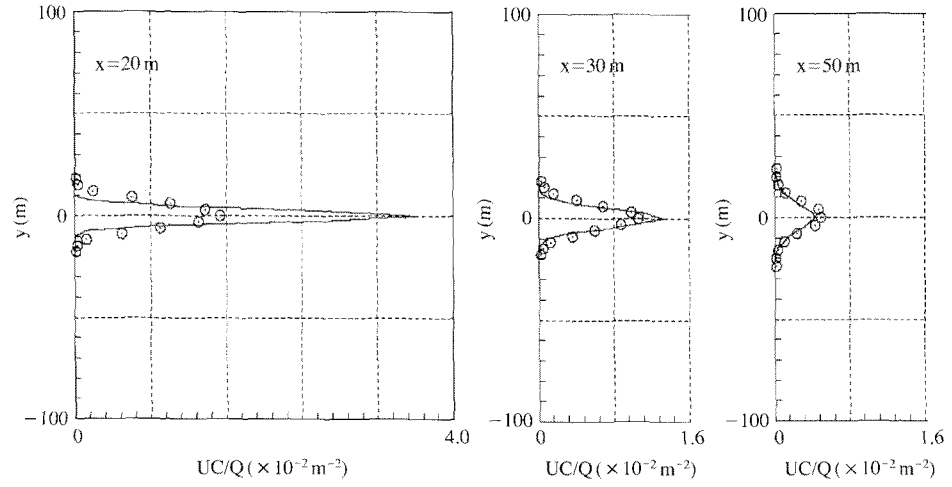

Fig. 7. As Fig. 6(a) but for lateral mean concentration at z=20 m.

A reversed flow, indicated by negative values of wind velocity, was obtained behind the ridge crest near the ground at x=200 m, and a cavity region formed, as shown in Fig. 8(b). The reversed flow was not observed further from the ridge at x=900 m. These features of wind velocity were observed in both calculations

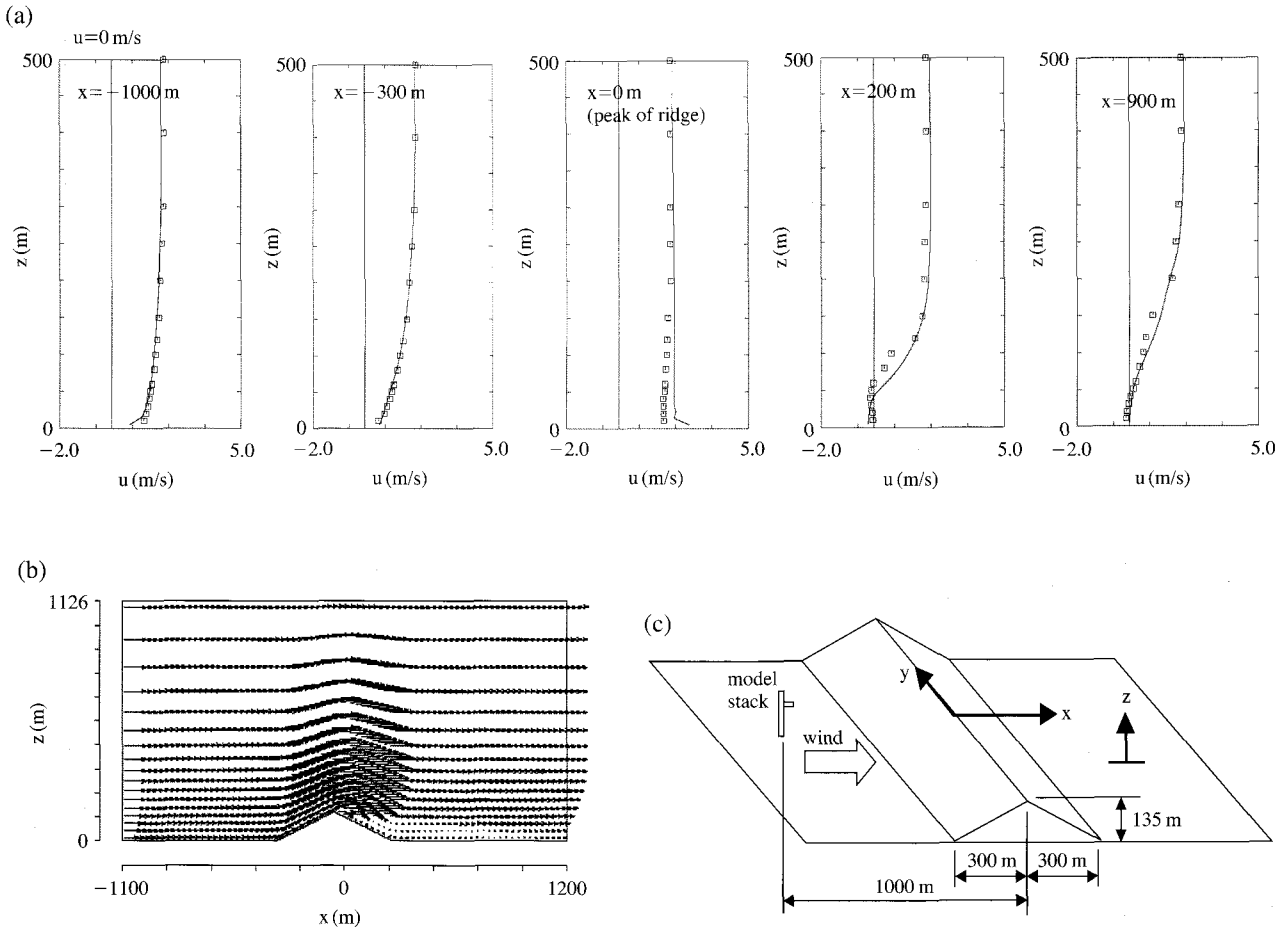

Fig. 8. (a) Mean velocity at y=0 m, the center position of the calculation domain. The solid lines and squares indicate the results of calculations and wind tunnel experiments, respectively. (b) Velocity vectors around the ridge at y=0 m. (c) Configuration of the ridge terrain.

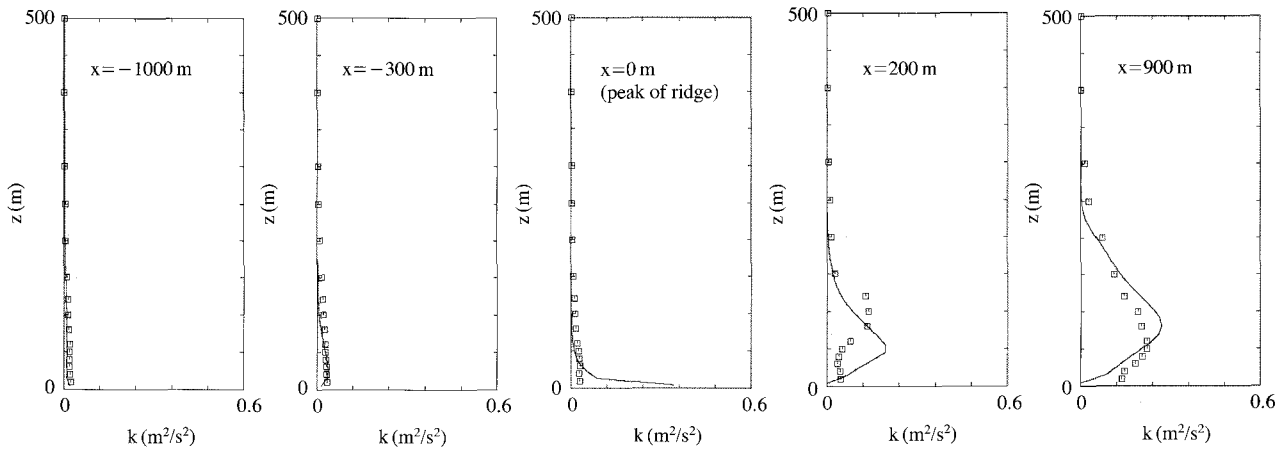

Fig. 9. As Fig. 8(a) but for turbulent kinetic energy.

and experiments.

Large calculated values of turbulent kinetic energy were obtained at the ridge crest at x=0 m, in the vicinity of the ground. This was because the terrain also

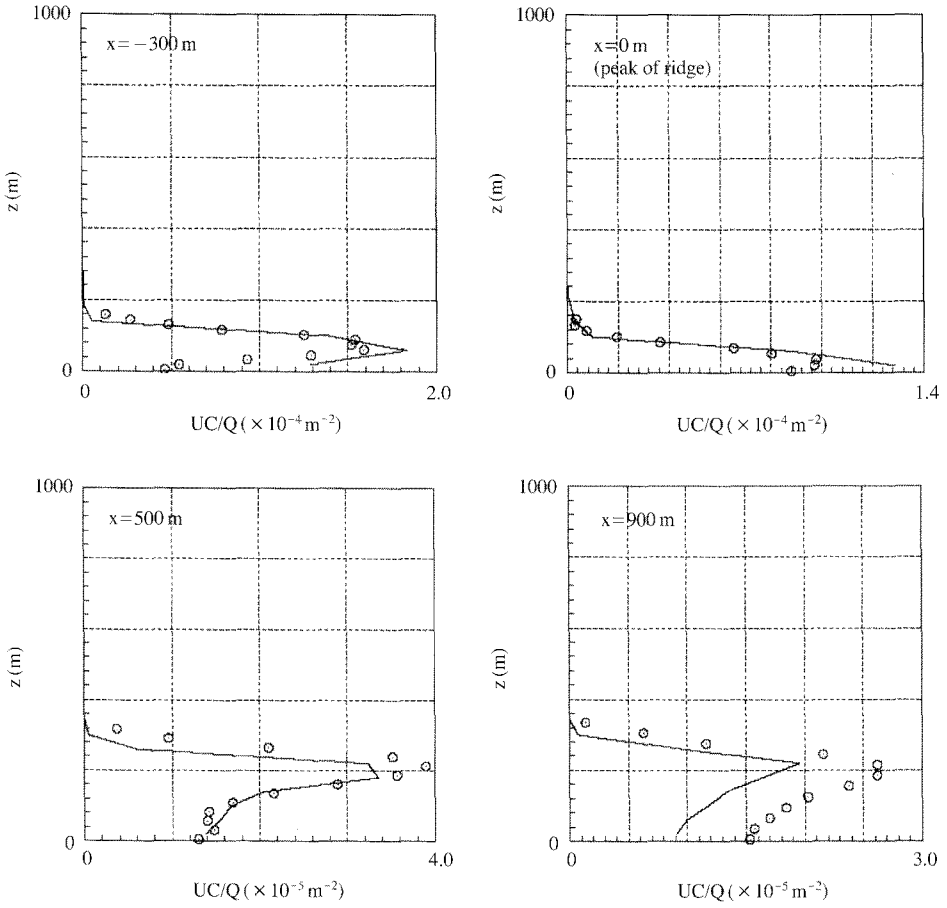

Fig. 10. Mean concentration at y=0 m, the center position of the calculation domain. The solid lines and circles indicate the results of calculations and wind tunnel experiments, respectively.

had a significant effect on the calculated turbulent kinetic energy results at x=0 m, similar to that on the velocity profile, as shown in Fig. 8. The increase in velocity at x=0 m in the vicinity of the ground caused the increase in velocity strain; thus, turbulent kinetic energy might also increase there. Large calculated values of turbulent kinetic energy were also obtained above the cavity region, viz., at elevated positions around z=50-100 m, behind the ridge at x=200 and 900 m. This was due to the large velocity gradient in the vertical direction due to the formation of the cavity region behind the ridge, and the production of turbulent kinetic energy might have occurred there. Although there were some discrepancies in the turbulent kinetic energy profiles, as mentioned above, calculated profiles were similar to those obtained from experiments, including those leeward of the ridge at x=200 and 900 m.

The calculated profiles of mean concentration in the vertical and lateral directions are shown in Figs. 10 and 11, respectively. Because the tracer gas was released at x=−1,000 m from an elevated source at z=50 m and transported under the flat-plate condition, the plume center in the vertical direction was calculated to be located at an elevated position at x=−300 m. At x=0 m, the tracer gas reached the ground and high values of concentration were detected there. High concentrations were also obtained at elevated positions behind the ridge at x=500 and 900 m, and this was because the tracer gas was transported at an elevated position and could not easily diffuse into the cavity region. This effect was estimated to be large in the calculation, and the concentrations near the ground at $z \leq 200$ m and x=900 m were smaller than those in experiments, as shown in Fig. 10. For these reasons, the calculated values of lateral concentration at $y \approx 0$ m and x=900 m, as shown in Fig. 11, were also smaller than those in experiments. Despite some discrepancies between the calculations and experiments, they were generally in good agreement.

5. CONCLUSION

A numerical simulation method based on the turbulence closure technique for atmospheric flow and the

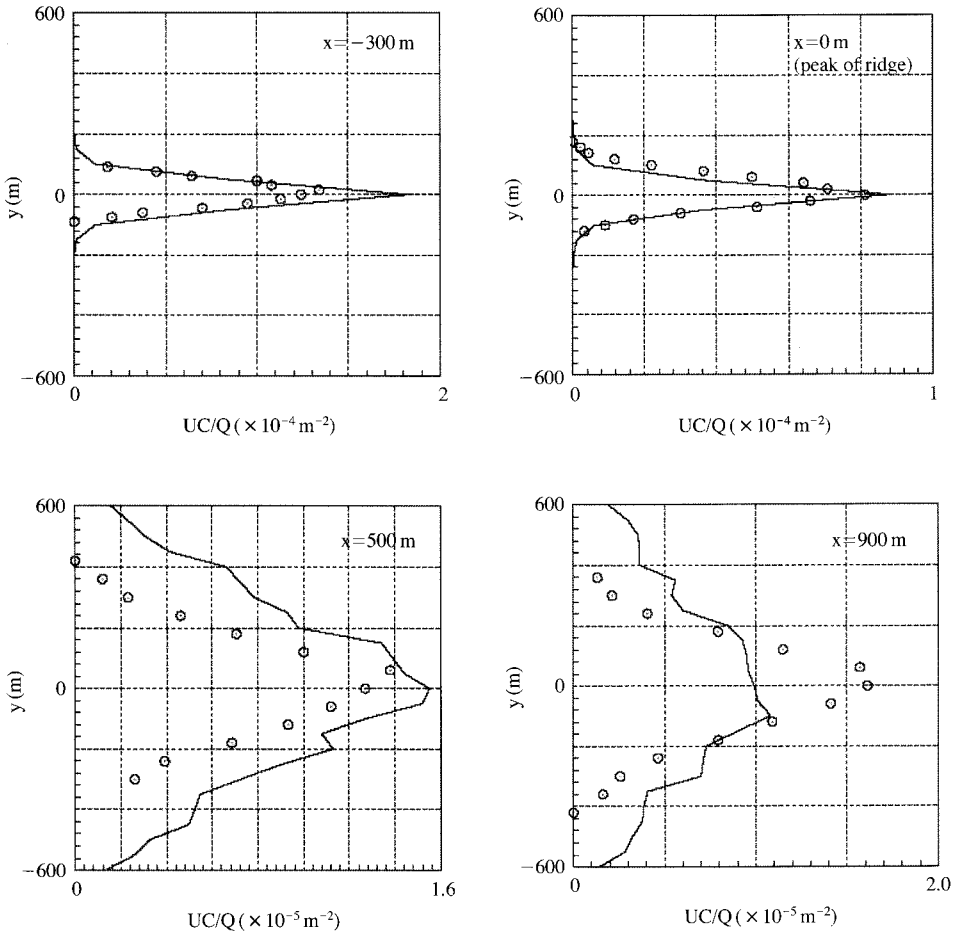

Fig. 11. As Fig. 10 but for lateral mean concentration at z=50 m.

Lagrangian particle model for stack gas diffusion in the atmosphere has been developed. Before applications of the model to actual complex terrains containing buildings, this model was separately applied to a single cubical building and to a two-dimensional ridge terrain in this study. Some discrepancies of calculation results were, for instance, obtained for the small lateral plume spreads under the flat-plate condition when compared with so-called P-G chart (in the Fig. 2), the small calculated turbulent kinetic energy in the vicinity of the ground surface and building roof (in the Fig. 4) and, further, small calculated tracer gas concentration (in the Fig. 10 at x=900 m). However, the calculated flow and stack gas diffusion results were compared with those obtained by wind tunnel experiments, and good agreement between the results of the calculation and the experiment were obtained for both wind velocity and stack gas concentrations, even though relatively coarse calculation grids were adopted around the building in this study. Dependence of the simulation accuracy on the grid resolution will be examined in the further studies where the model will be applied to the actual terrain containing buildings.

NOMENCLATURE

A_i^{α} : tensor of coordinate transformation $\left(=\frac{\partial \xi^{\alpha}}{\partial x^i}\right)$

a^i : coefficient of particle motion

b^{ij} : coefficient of random motion

C_{μ}, $C_{1\varepsilon}$, $C_{2\varepsilon}$, σ_k, σ_{ε} : model constants (=0.09, 1.44, 1.92, 1.0, 1.4, respectively)

C_{μ}^* : model constant in modified k-ε model

C_0 : model constant in diffusion model

g_a : density function of released particles

J : Jacobian of coordinate transformation

k : turbulent kinetic energy

n : unit vector normal to ground and building surface in vector notation

P : pressure

P_k : production term of turbulent kinetic energy transport equation ($=\nu_t S^2$)

Q : source strength
S : shear strain rate scale

$$\left(=\sqrt{\frac{1}{2}\left(\frac{\partial u_i}{\partial \xi^\alpha}\frac{\partial \xi^\alpha}{\partial x^j}+\frac{\partial u_j}{\partial \xi^\alpha}\frac{\partial \xi^\alpha}{\partial x^i}\right)^2}\right)$$

t : time
U : mean velocity in calculation domain, free stream velocity
u : mean velocity in physical domain ($=u_i$)
u_* : friction velocity
U : mean Eulerian velocity in vector notation ($=U^i$)
V : the Reynolds stress in vector notation ($=V^{ij}$)
u : velocity of released particle in vector notation ($=u^i$)
x^i : coordinate in physical domain (x streamwise, y lateral and z vertical)
x : position of released particle in vector notation ($=x^i$)
z_0 : roughness of ground and building surface ($=10$ cm)
ε : dissipation rate of turbulent kinetic energy
ξ^α : coordinate in calculation domain
κ : von Karman constant ($=0.4$)
ν : viscosity of air
ν_t : eddy viscosity
σ_y, σ_z : plume spreads in y and z directions
Ω : vorticity scale

$$\left(=\sqrt{\frac{1}{2}\left(\frac{\partial u_i}{\partial \xi^\alpha}\frac{\partial \xi^\alpha}{\partial x^j}-\frac{\partial u_j}{\partial \xi^\alpha}\frac{\partial \xi^\alpha}{\partial x^i}\right)^2}\right)$$

REFERENCES

Gross G. and F. Wippermann (1987) Channeling and countercurrent in the upper Rhine Valley: Numerical simulations. J. Climate and Applied Met., 26(10), 1293-1304.

Henn D.S. and R.I. Sykes (1992) Large-eddy simulation of dispersion in the convective boundary layer. Atmos. Environ., 26A(17), 3145-3159.

Ichikawa Y. and K. Sada (2001) A method of evaluating the topographical effect on atmospheric dispersion using a numerical model. Int. J. Environ. and Pollution, 16, 439-450.

Ichikawa Y. and K. Sada (2002) An atmospheric dispersion model for the environmental impact assessment of thermal power plants in Japan-A method for evaluating topographical effects. J. Air & Waste Manage. Assoc., 52, 311-323.

Kakishima S., K. Kayoiji, M. Nakai, S. Senshu, R. Ohba, and S. Nishijima (1985) Studies on wind tunnel experiments for safety analysis of a nuclear reactor, Energy & Environment Lab. Rep. (in Japanese), No. 219, pp. 13-14, 53-60.

Luhar A.K. and R.E. Britter (1989) A random walk model for dispersion in inhomogeneous turbulence in a convective boundary layer. Atmos. Environ., 23, 1911-1924.

Mengelkamp H.T. (1991) Boundary layer structure over an inhomogeneous surface: Simulation with a non-hydrostatic mesoscale model. Boundary-Layer Met., 57, 323-341.

Murakami S. (1997) Overview of turbulence models applied in CWE-1997, 2nd European & African Conference in Wind Engineering, Genova, Italy.

Murakami S., R. Ooka, A. Mochida, S. Yoshida, and S. Kim (1998) CFD Analysis of wind climate from human scale to urban scale. In Proceedings of Inter. Workshop on CFD for Wind Climate in Cities, Hayama, Japan, pp. 1-19.

Pasquill F. (1974) Atmospheric Diffusion. (2nd Ed.), John Wiley & Sons, pp. 365-380.

Sada K. (1996) Wind tunnel experiment on flow and tracer gas diffusion in convective planetary boundary layer. JSME Int. J., Series B, 39(1), 19-27.

Sada K. and A. Sato (2002) Numerical calculation of flow and stack-gas concentration fluctuation around a cubical building. Atmos. Environ., 36, 5527-5534.

Sada K., T. Michioka, and Y. Ichikawa (2006) Numerical simulation of atmospheric flow and stack gas diffusion under building and complex terrain conditions (Estimations of effective stack height and comparisons with wind tunnel experiments). JSME Int. J., Series B, 49(1), 48-59.

Takakura S., Y. Suyama, and M. Aoyama (1993) Numerical simulation of flowfields around building in an urban area. J. Wind Eng. & Industrial Aerodynamics, 46-47, 765-771.

Thomson D.J. (1987) Criteria for the selection of stochastic models of particle trajectories in the turbulent flows. J. Fluid Mech., 180, 529-556.

Tsuchiya M., S. Murakami, A. Mochida, K. Kondo, and Y. Ishida (1997) Development of a new k-ε model for flow and pressure fields around bluff body. J. Wind Eng. & Industrial Aerodynamics, 67 & 68, 169-182.

Weil J.C. (1990) A diagnosis of the asymmetry in top-down and bottom-up dispersion using a lagrangian stochastic model. J. Atmos. Sci., 47, 501-515.

Yamada T. and S. Bunker (1988) Development of a nested grid, second moment turbulence closure model and application to the 1982 ASCOT brush creek data simulation. J. Applied Met., 27(5), 562-578.

Yoshizawa A., S. Murakami, T. Kobayashi, N. Taniguchi, Y. Dai, and A. Kuroda (1995) Analysis of turbulent flows (in Japanese), Univ. of Tokyo Press, pp. 193-194.

(Received 16 May 2008, accepted 25 July 2008)